Drivers of Snowfall Accumulation in the Central Idaho Mountains Using Long-Term High-Resolution WRF Simulations

MIKELL WARMS,[a] KATJA FRIEDRICH,[a] LULIN XUE,[b] SARAH TESSENDORF,[b] AND KYOKO IKEDA[b]

[a] *Department of Atmospheric and Oceanic Sciences, University of Colorado Boulder, Boulder, Colorado*
[b] *Research Applications Laboratory, National Center for Atmospheric Research, Boulder, Colorado*

(Manuscript received 14 March 2023, in final form 26 June 2023, accepted 31 July 2023)

ABSTRACT: The western United States region, an economic and agricultural powerhouse, is highly dependent on winter snowpack from the mountain west. Coupled with increasing water and renewable electricity demands, the predictability and viability of snowpack resources in a changing climate are becoming increasingly important. In Idaho, specifically, up to 75% of the state's electricity production comes from hydropower, which is dependent on the timing and volume of spring snowmelt. While we know that 1 April snowpack is declining from SNOTEL observations and is expected to continue to decline as indicated by GCM predictions, our ability to understand the variability of snowfall accumulation and distribution at the regional level is less robust. In this paper, we analyze snowfall events using 0.9-km-resolution WRF simulations to understand the variability of snowfall accumulation and distribution in the mountains of Idaho between 1 October 2016 and 31 April 2017. Various characteristics of snowfall events throughout the season are evaluated, including the spatial coverage, event durations, and snowfall rates, along with the relationship between cloud microphysical variables—particularly liquid and ice water content—on snowfall amounts. Our findings suggest that efficient snowfall conditions—for example, higher levels of elevated supercooled liquid water—can exist throughout the winter season but are more impactful when surface temperatures are near or below freezing. Inefficient snowfall events are common, exceeding 50% of the total snowfall events for the year, with some of those occurring in peak winter. For such events, glaciogenic cloud seeding could make a significant impact on snowpack development and viability in the region.

SIGNIFICANCE STATEMENT: The purpose and significance of this study is to better understand the variability of snowfall event accumulation and distribution in the Payette Mountains region of Idaho as it relates to the local topography, the drivers of snowfall events, the cloud microphysical properties, and what constitutes an efficient or inefficient snowfall event (i.e., its ability to convert atmospheric liquid water into snowfall). As part of this process, we identify how many snowfall events in a season are inefficient to determine the number of snowfall events in a season that are candidates for enhancement by glaciogenic cloud seeding.

KEYWORDS: Snowfall; Snowpack; Cloud microphysics; Regional models; Cloud seeding

1. Introduction

As water and renewable electricity demands increase and climate change alters the predictability and seasonal variability of precipitation in many regions globally (O'Gorman 2014), accurately predicting changes to the accumulation and distribution of wintertime snowfall in mountainous regions (Livneh and Badger 2020) has become an area of significant concern. The western United States, in particular, is highly dependent on winter snowpack from the mountain west (Dettinger et al. 2015), as meltwater from winter snowpack provides crucial water resources for agriculture and individual use, hydroelectric power, as well as for fishing and tourism. All of these industries are vital for the economy of Idaho, and as much as 50% of Idaho's internally produced electricity—down from 75% in 2016—comes from hydroelectric power plants whose efficiency is dependent on spring and summer runoff timing and volumes (U.S. Energy Information Administration 2022, 2016). Understanding the seasonal variability of accumulation and distribution of snowfall in Idaho is vital for anticipating water supply challenges. To combat snowpack variability and improve water security in Idaho and other mountainous regions globally, orographic glaciogenic cloud seeding has been used as a mitigation tool despite the uncertainties in its efficacy (Rauber et al. 2019).

Observations of Snowpack Telemetry (SNOTEL) sites and streamflow gauges indicate that 1 April snow water equivalent (SWE) at snow courses across the mountain west have declined (Mote et al. 2005; National Water and Climate Center 2022) and spring runoff has trended earlier (Stewart et al. 2005; Dudley et al. 2017) over the past several decades. To quantify the effects of climate change on snowpack, regional and global climate models have been evaluated for their ability to reproduce snowpack evolution (Rasmussen et al. 2011; Chen et al. 2014). While most climate model forecasts agree that 1) temperatures are likely to continue to increase in the mountain west, 2) winter precipitation is likely to decline as a whole, and 3) the seasonal variability of winter precipitation and runoff volumes and timing is likely to increase, certainty

Supplemental information related to this paper is available at the Journals Online website: https://doi.org/10.1175/JAMC-D-23-0050.s1.

Corresponding author: Mikell Warms, mikell.warms@colorado.edu

DOI: 10.1175/JAMC-D-23-0050.1

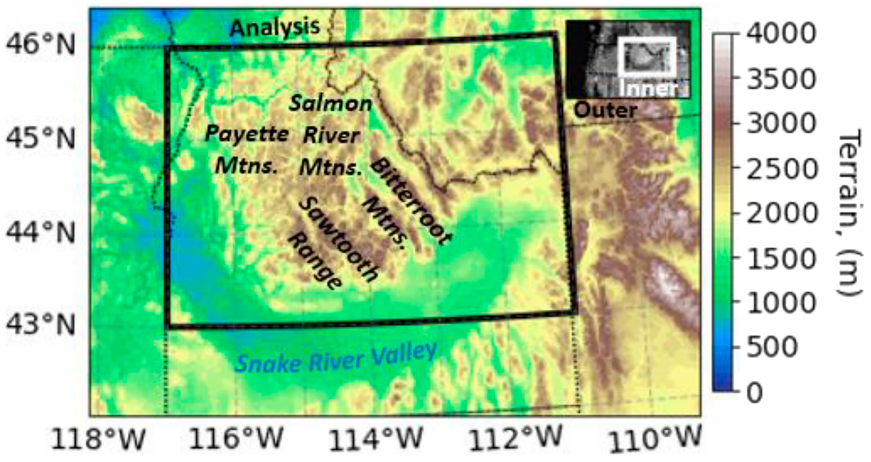

FIG. 1. Topographic map showing the WRF Model inner domain and the analysis domain over the mountains of central Idaho (black-outlined box). The outer domain is shown in the upper-right corner with an outline of the WRF Model inner domain.

in changes to snowfall amounts at the regional scale is less robust (Kharin et al. 2013).

In the Intermountain West and Idaho, more research is needed to understand the complex interplay of the drivers of snowfall accumulation and distribution. Recently, attention has been given to the pathways by which moisture travels from the Pacific Ocean to the Intermountain West (Alexander et al. 2015; Rutz et al. 2014) and their importance on snowfall within the Payette Mountains of western Idaho (Cann and Friedrich 2020). Less attention has been given to early and late season snowfall in the Intermountain West, the role of local topography, and the cloud microphysics affecting snowfall patterns in the region, which are addressed in this paper.

Enhancing snowpack through cloud-seeding operations has been an area of interest to stakeholders seeking to enhance water resources by modifying cloud microphysical properties, especially in mountainous regions. The goal of wintertime cloud seeding is to introduce ice nuclei in an area of enhanced supercooled liquid water (SLW) to boost the development of ice particles (mostly via riming and deposition) in snowfall-producing clouds (Ludlam 1955). Enhanced SLW can be advected or generated through orographic lift, convection, turbulence, or atmospheric instabilities (Rauber et al. 2019). Significant work has been carried out in the Payette Mountains of Idaho (Fig. 1) as part of the Seeded and Natural Orographic Wintertime Clouds: The Idaho Experiment (SNOWIE) project (Tessendorf et al. 2019) related to in situ cloud-seeding experimentation and analysis (French et al. 2018; Friedrich et al. 2020; Xue et al. 2022).

In this study, we attempt to answer the following questions: 1) What are the effects of the local topography on the distribution of snowfall in the region? 2) How do snowfall drivers and event characteristics evolve throughout the winter season? 3) What are the dominant mechanisms driving events that significantly impact snowpack growth? 4) What are the relationships between cloud microphysical variables—particularly liquid and ice water content—and snowfall accumulation? 5) Is it possible to identify the number of snowfall events that are candidates for cloud seeding?

To answer these questions, we use a 0.9-km-resolution hourly Weather Research and Forecasting (WRF) Model reanalysis of the 2016/17 winter season (October–April) of Idaho and its surrounding states (Fig. 1). The National Center for Atmospheric Research (NCAR)-generated model simulation was run as part of the SNOWIE project. The WRF Model output provides hourly snowfall accumulation and distribution, as well as moisture transport and cloud-microphysical variables for the entire winter season.

2. Model and methods

a. *SNOWIE-WRF Model, analysis domain, and model validation*

The WRF Model, version 3.9.1.1, was run in a continuous hourly simulation from 1 October 2016 to 30 April 2017 (Tessendorf et al. 2019). Initial and boundary conditions were obtained from the European Centre for Medium-Range Weather Forecasts ERA-Interim dataset (31-km horizontal resolution; ECMWF 2011). WRF was run with a large outer domain of coarser resolution (2.7-km horizontal resolution) including much of the Pacific Northwest (approximately from 39° to 49°N and from 105° to 128°W) and a nested inner domain with 0.9-km horizontal resolution covering southern and central Idaho (approximately from 42° to 46°N and from 109° to 118°W) (Fig. 1).

Vertically, WRF was run with 81 terrain-following levels between the surface and 20 hPa, with atmospheric levels distributed more densely at lower elevations. WRF parameterization schemes included the Thompson and Eidhammer aerosol-aware microphysics scheme (Thompson and Eidhammer 2014), the Mellor–Yamada Nakanishi and Niino 2.5 planetary boundary layer scheme (Nakanishi and Niino 2006), the Noah-MP land surface model (Niu et al. 2011), and the Rapid Radiative Transfer Model (RRTMG; Iacono et al. 2008).

The analysis domain for this study is a truncated portion of the higher 0.9-km-resolution inner domain over the central Idaho mountains (from 43° to 46°N and from 111° to 117°W) (Fig. 1). The total area of the analysis domain is approximately 160 000 km^2, with 73.5% of the domain exceeding an elevation 1.5 km, 37.9% of the domain exceeding 2 km, and 8.4% of the domain exceeding 2.5 km. The maximum and minimum elevations within the domain are 3445 and 377 m MSL, respectively.

The ability of the WRF Model to reproduce seasonal snowfall and snowpack has been successfully demonstrated (Rasmussen et al. 2011; Liu et al. 2016); however, model evaluation of the seasonally accumulated snowfall at several SNOTEL stations was conducted as part of SNOWIE. The WRF Model satisfactorily reproduces seasonal snowpack evolution, consistently underpredicting precipitation 10% or less and adequately capturing the spatial distribution of snowfall in comparison with observations (appendix; Tessendorf et al. 2018).

b. *Analysis methods*

1) Precipitation accumulation and distribution

The seasonal precipitation analysis centers on the distribution and accumulation of snowfall and rainfall within the domain. The statistics include the total accumulated precipitation at each grid cell and the domain-averaged hourly snowfall and rainfall accumulation throughout the season, which does not account for ablation, melting, or sublimation/evaporation. Temporal evolution of snow and rainfall accumulations are also averaged over the entire analysis domain and excluding grid cells below 1.5, 2, and 2.5 km MSL (referred to as elevation bands hereinafter).

Individual snow events between 1 October 2016 and 30 April 2017 are identified. An event is defined as continuous domain-averaged snowfall > 0.025 mm with less than 3 h of interruption (Barlow et al. 2019; Laiho et al. 2023). A total of 87 snowfall events were identified between 1 October and 30 April, and various statistics were calculated for each event grouped by month (mean, minimum, maximum, and standard deviation of event duration, total snowfall amount, and hourly snowfall rate).

2) Thermodynamics

The thermodynamics analysis focuses on the vertical structure of the atmosphere as it relates to freezing level, atmospheric stability, moisture, and water vapor transport within the analysis region on average during each month and the 87 identified snowfall events. Hourly atmospheric temperature T and equivalent potential temperature θ_e were averaged for each month for all times and for times during snowfall events. Integrated water vapor transport (IVT) was calculated at each grid cell over all atmospheric levels using pressure p, specific humidity q, and wind $\mathbf{V}$:

$$\mathrm{IVT} = \int_{1000\mathrm{hPa}}^{20\mathrm{hPa}} q\mathbf{V}\, dp. \tag{1}$$

IVT has been reasonably well correlated ($r \sim 0.6$) with wintertime precipitation in the mountain west (Rutz et al. 2014; Cann and Friedrich 2020). Weather systems with IVT > 250 kg m^{-1} s^{-1} approaching the West Coast are often referred to as atmospheric rivers (Rutz et al. 2014; Ralph et al. 2019). Atmospheric rivers with stronger winds and higher moisture content (i.e., higher IVT)—typically occurring between November and February—can penetrate farther inland and provide moisture to the central Idaho mountains (Rutz et al. 2014; Cann and Friedrich 2020). Monthly maximum IVT and monthly average event-based IVT are calculated to determine moisture fluxes within the analysis domain. This approach can also exhibit the moisture pathways of water vapor as they approach the Idaho mountains and are either orographically lifted and transitioned to precipitable water at the higher elevations or tend to veer around the mountainous obstructions. These differing pathways can be seen by upper-level wind patterns (Fig. S1 in the online supplemental material), higher levels of IVT in the low-lying Snake River plane, or through a reduction of IVT at higher elevations (Fig. 7, below).

3) Cloud microphysics of events

In addition to water vapor transport, we analyze the relevant WRF cloud microphysics output variables (cloud, rain, ice, snow, and graupel mixing ratios) during events as they relate to seasonality and event efficiency. Total liquid water content (LWC) in grams per meter cubed at a given location is defined as the sum of rain and cloud mixing ratios multiplied by the moist air density; and total ice water content (IWC) in grams per meter cubed is defined as the sum of the ice, snow, and graupel mixing ratios multiplied by the moist air density. Averages of LWC and IWC at each modeled atmospheric level were calculated during each event.

SLW, defined as LWC when $T < 0$°C, is an important metric for snowfall production and cloud-seeding potential (Rauber et al. 2019) as it can result in riming—an efficient method with which to enhance snow crystal growth (Mitchell et al. 1990; Rauber and Grant 1986). Enhanced SLW is often found in orographic updrafts, mountain induced gravity waves, cloud-top generating cells, Kelvin–Helmholtz billows, and turbulent shear zones (Rauber et al. 2019). In this study, we use column-integrated SLW and IWC content metrics to analyze their relative magnitudes during events. The event-based SLW and IWC are then correlated with snowfall accumulation per event.

Similarly, the ratio of SLW to IWC was examined as a proxy for riming efficiency. In theory, a lower ratio of SLW to IWC during a snowfall event reveals that the event 1) is inefficient at riming (perhaps due to a dearth of ice nuclei or poor mixing between atmospheric levels) or 2) has a relatively warm atmosphere or 3) has small amounts of SLW available, and thus ice crystal formation is more closely related to other processes such as nucleation and deposition.

3. Results with discussion

a. *Precipitation accumulation and distribution*

The highest snowfall accumulations within the analysis domain (>1.2 m) occurred on the western and central slopes of

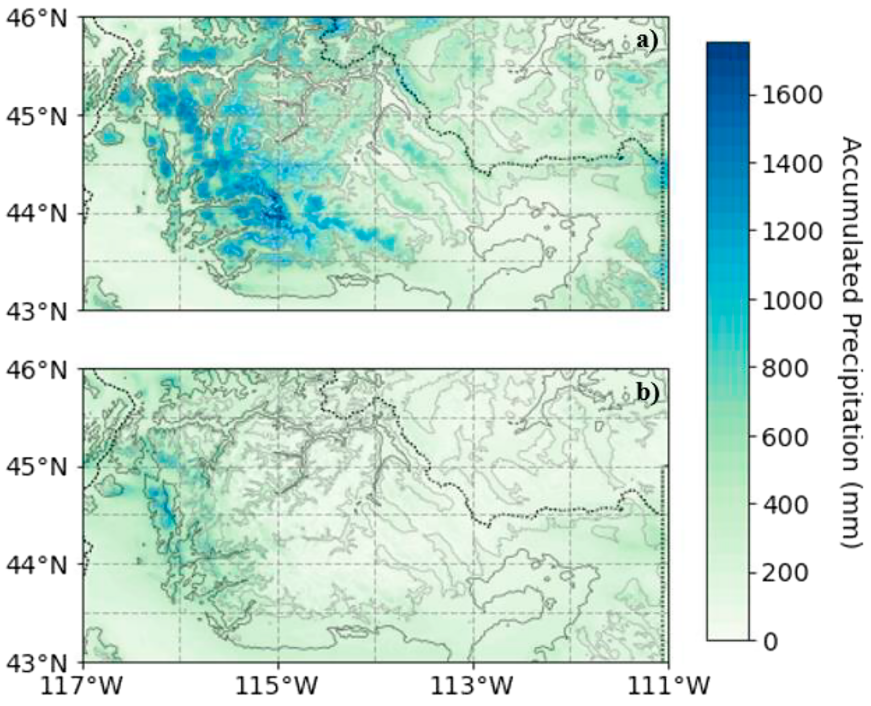

FIG. 2. Total (a) snowfall and (b) rainfall accumulation between 1 Oct 2016 and 30 Apr 2017 over the analysis domain. Black dotted lines indicate state lines. Underlying terrain is indicated by 1500- (black), 2000- (gray), and 2500-m (white) contour lines.

the Payette Mountains, parts of the western Salmon River Mountains, and over the Sawtooth Range with a maximum snowfall accumulation of 1.7 m falling on the largest peaks (>3 km) (Fig. 2a). In contrast, the Bitterroot Mountains east of the Sawtooth Range and the eastern Salmon River Mountains do not receive nearly as much snowfall (maximum < 1 m) because at least 80% of all precipitation events in January–March of 2017 in the region are driven by moisture fluxes from the west and southwest (Cann and Friedrich 2020). The lower elevation areas (<1.8 km) in central Idaho including the Snake River valley receive less than 0.5 m of total precipitation as snowfall.

The highest rainfall accumulations (>0.8 m) occur in the westernmost Payette Mountains (between 2 and 2.5 km MSL; Fig. 2b). Moderate rainfall accumulations (0.3–0.8 m) occurred in the rest of the Payette Mountains and the western Salmon River Mountains and Sawtooth Range. Elsewhere in the analysis domain including the Snake River valley, the Bitterroot Mountains, and the eastern Sawtooth Range and Salmon River Mountains, rainfall accumulations are typically less than 0.3 m (Fig. 2b). At the highest elevations (>2.5 km), minimal rainfall occurs as a result of colder temperatures during the simulated months (average atmospheric temperatures are below 0°C at 2.5 km during all months except October; Fig. 5 below), and a similar westerly flow (Fig. S1 in the online supplemental material) effect is causing the lack of rainfall in the eastern mountain ranges. The sparse spatial distribution of rainfall accumulation in the region speaks to the importance of winter snowfall accumulations for water resources in Idaho.

The majority (almost 90%) of snowfall from the 2016/17 winter season in the analysis domain occurred in December–April, with smaller accumulations in October–November. A rain and snow mixture was present during October through early November when almost all rain ceased until mid-February (<25 mm of rainfall occurred during that period), slowly increasing as temperatures warmed in the spring (Fig. 3). The total domain-averaged snowfall between 1 October and 30 April was 365 mm, with larger average snowfall at higher elevations (>1.5 km MSL). If grid cells below 1.5, 2, and 2.5 km MSL are excluded, those domain averages increase to 436, 559, and 680 mm, respectively. The domain-averaged rainfall between 1 October and 30 April was 226 mm, and excluding grid cells below 1.5, 2, and 2.5 km MSL results in those domain averages decreasing to 205, 169, and 123 mm, respectively (Fig. 3).

b. *Snowfall event statistics*

Whereas section 3a provides a top-level view of the spatiotemporal evolution of precipitation within the domain, we now analyze the frequency, duration, variability, and strength of all snowfall events that occurred in the 2016/17 winter season (Table 1). Of the 87 snowfall events identified, 28 (32% of total) occurred in October and November (ON) totaling only 11% of the seasonal snowfall accumulation. Much of the precipitation during these months fell as rainfall (86 mm) as opposed to snowfall (43 mm). Events in October and November were, on average, respectively 14 and 8 h shorter than the annual mean of 26.6 h and less variable in duration, with a

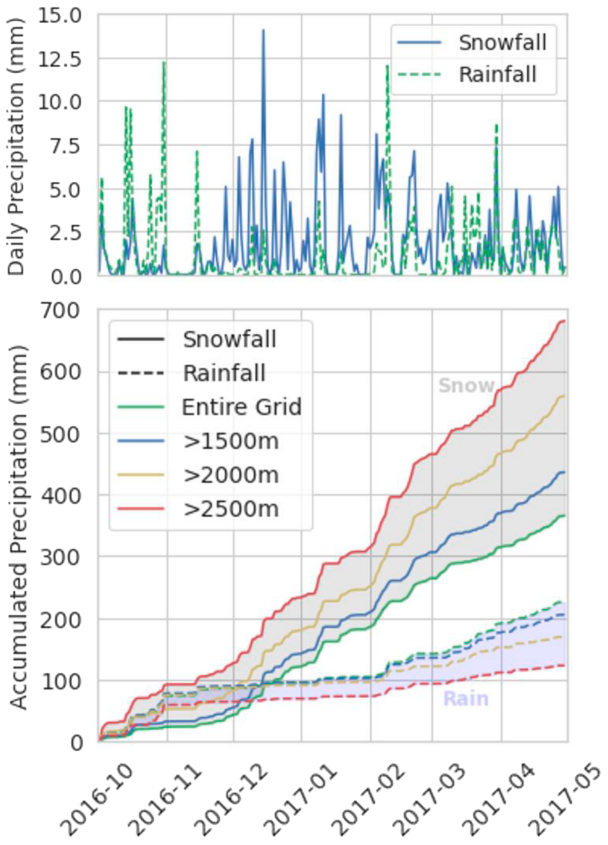

FIG. 3. (top) Domain-averaged daily snowfall and rainfall. (bottom) Domain-averaged snow (solid) and rain (dashed) accumulation for the entire domain (green) and for the domain excluding grid cells below 1.5 (blue), 2 (yellow), and 2.5 (red) km MSL. Shading indicates the difference between the entire domain average and the domain excluding grid cells below 2.5 km MSL.

standard deviation of 10.5 and 12.6 h, respectively, as opposed to the annual standard deviation of 30.2 h. The domain-averaged mean event snowfall for October (21.8 mm) and November (18.4 mm) was also much lower than for the annual average (50.7 mm). In addition, less of the domain received snowfall from each event during October (21.4%) and November (34.9%) relative to the annual mean (37.8%). In October, most of the snowfall occurred at higher elevations as the spatial snowfall coverage increased from 21.4%, 28.4%, 42.6% to 57.1% for the grid cells in the domain to those above 1.5, 2, and 2.5 km MSL, respectively.

Over 60% of the seasonal snowfall accumulation occurs between December and February (DJF), with fewer events and a larger variability in total event accumulations relative to October, November, March, and April (Table 1; Fig. 4). The snowfall events durations in December (30.3 h), January (29.4 h), and February (52.3 h) are 3.7, 2.8, and 23.7 h longer than the seasonal average (26.6 h), respectively, with February having the longest average event durations of any month by over 20 h. DJF also had larger and more widespread event snowfall, receiving domain-averaged snowfall amounts of 75.9, 63.1, and 77.7 mm, with a domain areal coverage of 63.1%, 54.5%, and 47.4%, respectively. With largely subfreezing temperatures over the entire analysis domain, snowfall in DJF was observed at all elevations—see section 3c for a discussion of event temperatures. In December, an average of 63.1% of the domain saw snowfall accumulations during events (i.e., 36.9% of the domain was dry—likely—or had precipitation fall as rainfall) as compared with 67.5%, 73.1%, and 75% above 1.5, 2, and 2.5 km MSL, respectively.

March and April (MA) combined had 27 identified snow events (31% of total), accumulating slightly less snowfall per event (3.3–4.1 mm) than DJF (5.3–8.6 mm) but much more than ON (1.3–1.7 mm). With a total of 48.9 and 49.8 mm of domain-averaged snowfall, respectively, March and April were close to the annual monthly average of 50.7 mm. MA account for 28% of the total seasonal accumulation with event durations (25.6–29.8 h) also close to the annual average of 26.6 h for the 2016/17 winter season (Table 1). For April, most of the snow fell on the higher terrain with only 27.9% of the domain receiving snowfall during events on average as compared with 35.8%, 48.5%, and 55.6% above 1.5, 2, and 2.5 km MSL, respectively.

c. *Thermodynamics*

The mean atmospheric temperature profiles during snowfall events (Fig. 5a) show a relatively stratified atmosphere during all months, only during the coldest month of January does the average event temperature profile hint at a small surface inversion or isothermal surface layer. The lowest

TABLE 1. Monthly snowfall event characteristics between 1 Oct 2016 and 30 Apr 2017.

		Oct	Nov	Dec	Jan	Feb	Mar	Apr
No. of events		17	11	11	12	9	12	15
Event duration (h)	Mean	12.5	18.6	30.3	29.4	52.3	29.8	25.6
	Max	38	46	61	91	134	157	136
	Std dev	10.5	12.6	18.6	24.6	44.7	40.6	33.0
Grid-averaged snowfall per event (mm)	Mean	1.3	1.7	6.9	5.3	8.6	4.1	3.3
	Max	4.8	6.2	19.6	28.9	25.4	23.8	18.0
	Std dev	1.5	1.7	6.2	7.7	9.5	6.5	4.8
Percent of domain receiving snowfall	Mean	21.4	34.9	63.1	54.5	47.4	28.7	27.9
	Min	8.3	15.2	35.9	16	26.8	10.4	8.9
	Max	46.2	75	80.3	73.1	59.6	46.1	38.6
	Std dev	11.6	18.5	12.7	15.3	10.1	11.8	8.3

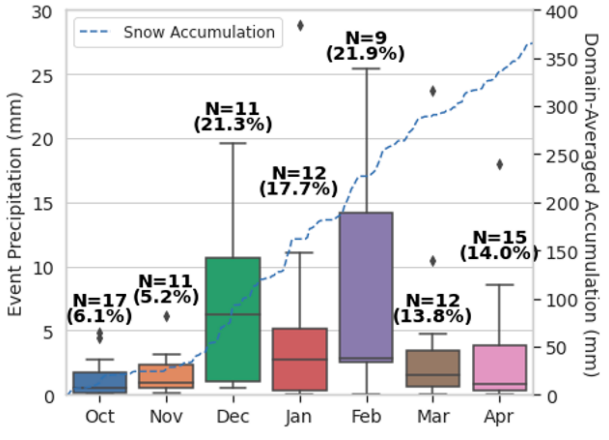

FIG. 4. Box-and-whiskers plot of median snowfall event accumulation between October 2016 and April 2017. The box represents 25%, 50%, and 75% percentiles, and the whiskers denote the 5% and 95% percentiles; outliers are shown as diamonds. Number of events and percentage of total seasonal snowfall are highlighted for each month. Total domain-averaged snowfall accumulation is shown as a blue dotted line.

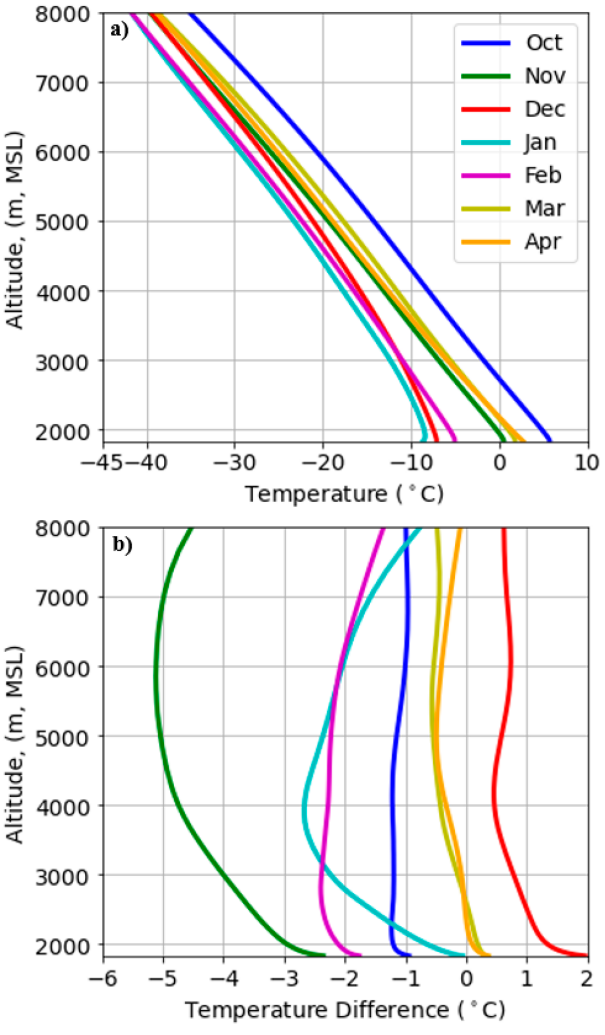

FIG. 5. (a) Domain-averaged monthly mean temperature profiles during snowfall events (mean event temperature). (b) Difference between domain-averaged mean event temperature and monthly mean temperature profiles for all times.

temperatures during events were observed in DJF, which corresponds with the highest monthly snowfall accumulations. November, March, and April (NMA) have similar average event temperature profiles, with November being slightly cooler (2.5°C) at the surface. Surface and lower atmosphere temperatures (between 2 and 3 km MSL—an important atmospheric region for snowfall) are mainly above 0°C in October, range between −8° and 2°C in NMA, and range between −12° and −5°C in DJF. October stands as an outlier in comparison with the other months, with average surface event temperatures exceeding 5°C and with only the highest peaks (>2.7 km) seeing freezing surface temperatures on average. Temperatures between −10° and −15°C, which favor the growth of dendritic ice particles (Takahashi et al. 1991; Fukuta and Takahashi 1999), and between −10° and −12°C, which favor maximum SLW (Rauber and Grant 1986), are found on average at 2.5–3.8 km in DJF, 3.5–4.8 in NMA, and 4.5–6.5 km in October.

Except for December and at lower elevations during MA, mean event temperatures below 8 km during snowfall events are, on average, colder than the monthly mean temperatures (Fig. 5b). In December, temperatures during snowfall events are warmer than the monthly mean temperature, and in MA temperatures between events and monthly mean are within ±0.5°C. Figure 3 shows that most November snowfall events occurred later in the month, making the mean event temperatures tend toward colder-than-average November temperatures. In January, while the surface temperature is similar between events and mean monthly temperatures, the event temperatures become much colder at height in the atmosphere, exceeding 2.5°C colder at 4 km MSL (Fig. 5b). Temperatures during October and February events are approximately 1° and 2°C colder, respectively. For all months, the minima of the temperature differences excluding higher elevations (>8 km) occurs at the surface. This indicates that the monthly average temperature profile and lapse rate in the boundary layer is more isothermal and perhaps slightly less stable than the average during events. For all months except November and January between 2.5 and 8 km MSL, the temperature differences are fairly constant, indicating average profiles within this region of the atmosphere are consistent during events and nonevents.

While the regional terrain provides lifting of moisture orographically, snowfall production can also be enhanced through lifting of moisture via atmospheric static instability, among other processes (Rauber et al. 2019). Domain-averaged event equivalent potential temperature θ_e profiles (Fig. 6a) for all months exhibit relative static stability (or neutrality) within the entire atmospheric column. DJF are more statically stable during events ($d\theta_e/dz \gg 0$) near the surface (<4 km MSL) than are October, November, March, and April (ONMA), which have a more neutral stability profile ($d\theta_e/dz \sim 0$). Relative

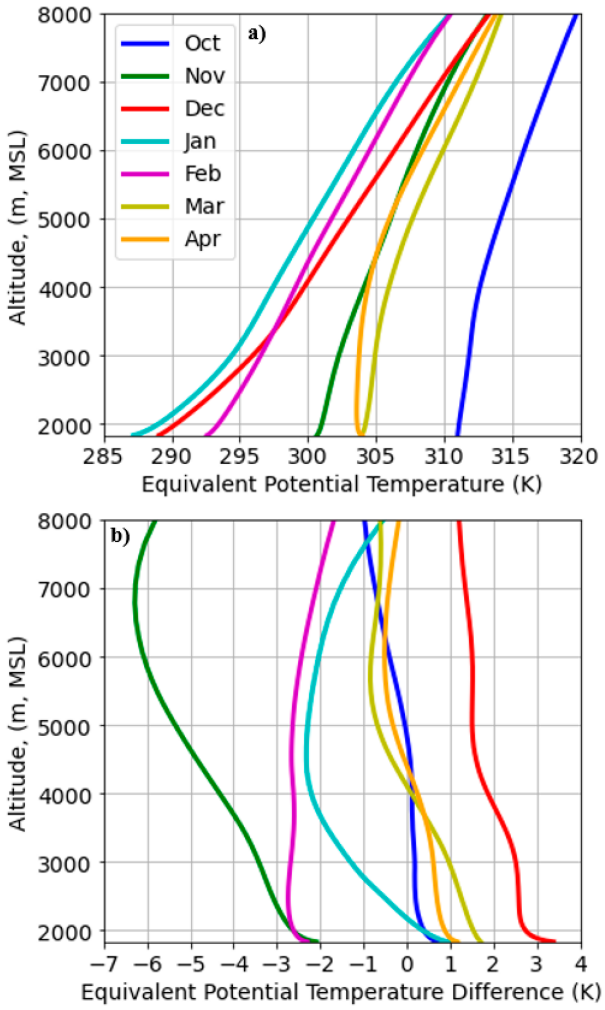

FIG. 6. As in Fig. 5, but showing the event-based equivalent potential temperature.

average event stability indicates that lifting of liquid water content required for snowfall is predominantly orographic or that the localized updraft instabilities that can occur in mountainous regions are averaged out. Mean event surface θ_e profiles have greater magnitude differences between the DJF and October (25 K) than do the average event temperatures (10 K) due to reduced moisture during events in DJF—see section 3d for discussion of moisture transport. Similar month groupings are seen in the mean θ_e profiles as to the mean event temperature profiles in Fig. 5a. Surface θ_e during events ranges from the 287 to 293 K for DJF, 301–304 K for NMA, and >310 K for October.

Except for February and November, mean surface θ_e during snowfall events for each month is, on average, 1–3 K higher than the corresponding mean monthly surface θ_e (Fig. 6b). Mean θ_e profile differences are very similar to the mean temperature profile differences. Any differences between the two figures signify differences in moisture and/or stability. The θ_e differences shown in Fig. 6b do not portray large differences in stability between events and nonevents. February and November are slightly more stable during events and the other months are slightly less stable during events during nonevents, at least near the surface.

As stated previously, IVT is reasonably well correlated with snowfall in central Idaho. Spatial distribution of average (Fig. 7; color contours) and maximum (Fig. 7; contour lines) monthly IVT during events indicates when and where high moisture transport occurs. In all months, the pattern of higher average event-based IVT occurs mainly on the western and southwestern edges of the domain, continuing eastward into the Snake River valley. IVT is reduced as the moisture moves eastward toward the mountains, either because the moisture-carrying winds tend to veer around the mountainous obstructions (Fig. S1 in the online supplemental material) and/or the moisture transforming into LWC or IWC as it is lifted orographically.

The months with the largest average IVT during events were October (131.1 kg m^{-1} s^{-1}), February (122.1 kg m^{-1} s^{-1}), and March (118.0 kg m^{-1} s^{-1}), with November (97.2 kg m^{-1} s^{-1}) and December (103.1 kg m^{-1} s^{-1}) closer to the annual average (103.8 kg m^{-1} s^{-1}). The months with the lowest average IVT during events are January (81.7 kg m^{-1} s^{-1}) and April (75.8 kg m^{-1} s^{-1}). However, monthly maximum IVT is not necessarily correlated with the corresponding average IVT. For example, while March has a higher average IVT, its maximum IVT only exceeds 400 kg m^{-1} s^{-1} in one small region. In January, the maximum IVT exceeds 500 kg m^{-1} s^{-1} west of the mountains—an elevated level that only occurs in two other months (October and February)—while its average IVT is fairly low. Other than October, DJF have the highest maximum IVT values (Fig. 7; contour lines)—the months that also receive the highest amount of snowfall—with the largest event of the season occurring in January. The maximum IVT contour lines in January do not extend into the Snake River valley as is the typical pattern, potentially signifying a relatively efficient transition of transported moisture to precipitation during that event.

d. *Liquid water content and snowfall*

The presence of SLW in clouds can be a catalyst for intense wintertime snowfall. In this section, we first discuss LWC during events between the surface and 8 km MSL and then emphasize the LWC at $T < 0$°C, that is, SLW (Fig. 8). During the 2016/17 winter season, LWC is highest in October and mid-March through April, with monthly average column-integrated LWC below 8 km MSL of >0.45 kg m^{-2} during events. In November–February (NDJF), that value is between 0.034 and 0.037 kg m^{-2}. Column-integrated LWC averages during individual events throughout the season ranges from 0.15 to 0.97 kg m^{-2} with the largest values (>0.6 kg m^{-2}) occurring during events in October and early April. Higher LWC is generally observed at between 3 and 7 km MLS during these months. During the peak winter months of December through February, column-integrated LWC values range from 0.15 to 0.57 kg m^{-2} and generally occur lower in the atmosphere (<6 km).

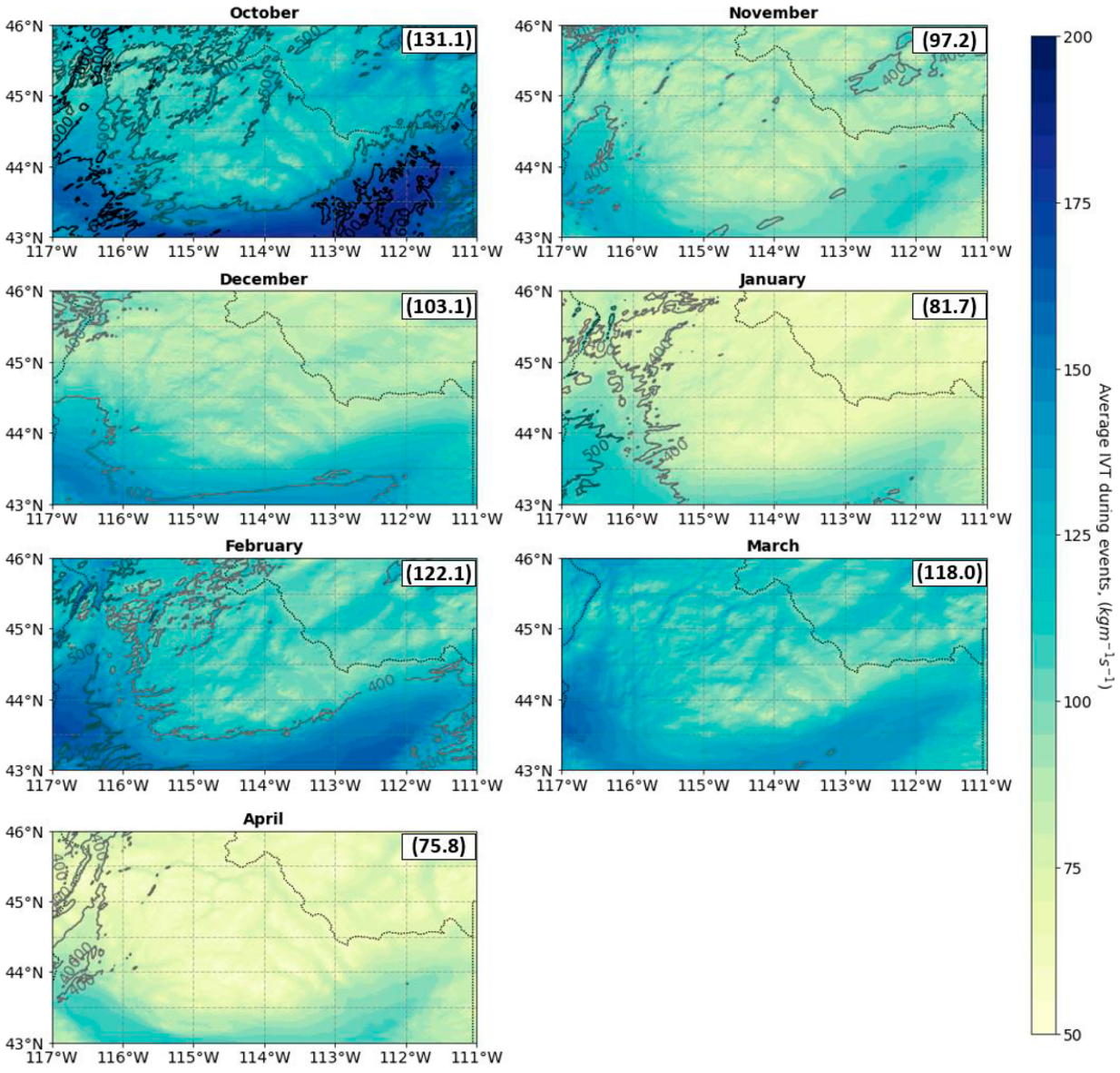

FIG. 7. Monthly average event-based (shading) and monthly maximum IVT (contour lines at 400, 500, and 600 kg m^{-1} s^{-1}). Monthly maximum IVT contour lines are not shown if IVT did not exceed 400 kg m^{-1} s^{-1} during that month (e.g., March). Monthly spatial averages are shown in the upper-right corner.

Freezing levels during snow events range between 2 and 3.5 km in October and early November, which is above the surface at lower terrain levels and near the surface of the highest peaks (Fig. 1). Cloud top heights can reach up to 13 km but are generally found between 7 and 10 km throughout the winter season. Much of late November into early March have average freezing levels near or at the surface, with March and April having average freezing levels between 2 and 3 km, slightly lower on average than October and early November. Despite the higher atmospheric freezing levels in October, March, and April, SLW (Fig. 8) follows the same seasonal pattern as does LWC. Average column-integrated SLW is lowest in NDJF (<0.37 kg m^{-2}), and slightly higher in OMA (>0.43 kg m^{-2}).

The domain areal coverage of liquid-containing columns (i.e., the percentage of domain area containing gridcell columns with liquid water path >0.2 g m^{-2}) during events (Fig. 8; dotted green line) varies from as low as 14% to as high as 82%. Orographic snowfall in the mountains can be advected, generated, or enhanced through multiscale dynamical processes such as orographic lift, mountain waves, cloud-top generating cells, and wind shear turbulence that are often linked to the underlaying terrain (Rauber et al. 2019). These dynamical features generate areas of enhanced updraft that can be a

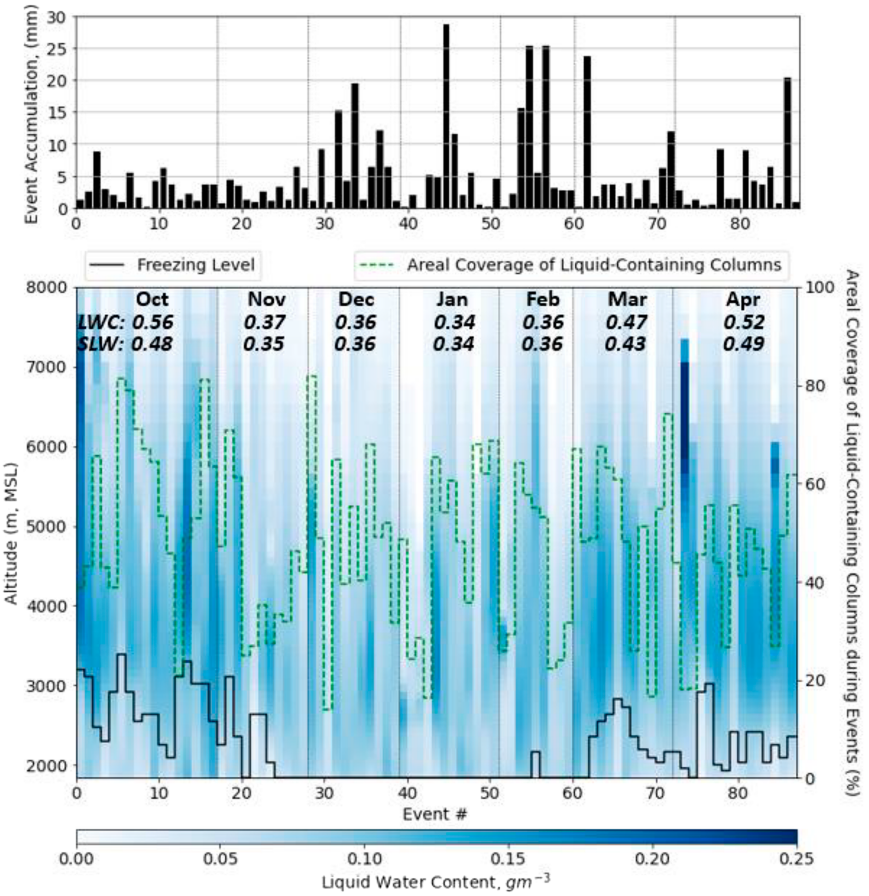

FIG. 8. (top) Spatially averaged snowfall accumulation per event averaged only where snowfall is occurring. (bottom) Domain-averaged LWC for each event as a function of height (shading) excluding grid cells with liquid water mixing ratios <0.001 g kg^{-1} below 8 km MSL (contains 95% of LWC). Domain and event-average height of the 0°C isotherm (solid black line), and areal coverage of liquid-containing clouds (dotted green line) are highlighted. LWC above the 0°C isotherm represents the available SLW. Monthly event average column-integrated LWC and SLW (kg m^{-2}) up to 8 km are shown as text values.

source of enhanced LWC at height in the atmosphere, which can be cooled and become SLW. Linking event-based SLW to the areal coverage of liquid water-containing clouds in this study is used as a proxy for determining if the LWC is widely generated through orographic lifting or if enhanced LWC originates from smaller-scale features. A higher event-average areal coverage suggests that a larger-scale frontal system is producing precipitation, whereas a smaller areal coverage could indicate localized snowfall activity from smaller-scale processes. The number of events in DJF that have an areal coverage of liquid-containing columns exceeding 50% of the domain is 15 (of 32 events). November only had 2 such events, whereas March and April had 7 and 4, respectively. Those events with higher areal coverages (>50%) tended to have higher average snowfall accumulations during DJF, whereas that pattern did not hold true with the warmer temperatures in MA. In general, regardless of the snowfall mechanism(s), the lower the areal coverage of liquid-containing columns in the domain is—even when coupled with higher SLW—the more likely it is that that event does not contribute significantly to the seasonal snowpack for the entire region as the snowfall will be more localized.

The question remains how efficiently LWC (or SLW) can be transformed into precipitation throughout the winter season by linking SLW to snowfall amounts, with an emphasis on the peak winter period of DJF. In DJF, the monthly event averages of column-integrated SLW are fairly similar at ~0.35 kg m^{-2} (Fig. 8). The number of events that have column-integrated SLW $>$ 0.04 kg m^{-2} in December–February is 3, 5, and 4, and the maximum column-integrated SLW for an event in each month are 0.51, 0.54, and 0.57 kg m^{-2}, respectively. However, while an event can have a high SLW content, that does not necessarily mean it will impact regional snowpack significantly. Whether it will depends highly on other factors, especially on the timing seasonally (i.e., temperature) and the ability of the cloud to transition SLW to IWC.

To illustrate the seasonal influence of SLW on snowfall amounts, the Pearson correlation coefficient r of column-integrated SLW and snowfall amounts for the entire season is 0.19 (significance level $p = 0.07$), while r increases to 0.52 ($p = 0.002$) for events in DJF only. However, there are a few events in December with high SLW that do not yield higher snowfall amounts: event 29 on 2 December and event 36 on 19 December have column-integrated SLW > 0.44 kg m^{-2} with high average areal coverage of liquid-containing columns of 81% and 68%; but they only lasted 12 and 19 h with spatially average snowfall amounts of 1.3 mm (0.11 mm h^{-1}) and 6.7 mm (0.5 mm h^{-1}), respectively. Neither of these two "high SLW" but shorter events in December accounted for the peak accumulation totals seen in other events in that month; however, the different snowfall rates of events 29 and 36 suggests that 36 was a more efficient event. In general, significant snowfall events seem to require a combination of 1) longer duration, 2) higher areal coverage of liquid-containing columns, and 3) higher-than-average SLW content. Events 32, 34, and 37 on 7, 13, and 22 December accounted for higher snowfall accumulation totals when compared with events 29 and 36. These higher event snowfall accumulations (15.4, 19.6, and 12.3 mm) are a function of their longer durations (53, 61, and 57 h), higher mean column-integrated SLW (0.044, 0.039, and 0.033 kg m^{-2}) and higher areal coverage of liquid-containing columns (64%, 55%, and 49%), yielding snowfall rates of (0.29, 0.32, and 0.22 mm h^{-1}) for the events, respectively.

Snowfall events in January, February, and early March display similar characteristics in SLW, snowfall rate, duration, and total accumulation to those in December, with a few heavy snowfall storms (events 45, 55, 57, and 62; Fig. 8) dominating the snowfall accumulation (28.8, 25.5, 25.5, and 23.9 mm). These events are much longer (91, 134, 127, and 157 h), have liquid-containing clouds covering larger areas (close to 50% of the domain), and have higher mean column-integrated SLW (0.47, 0.52, 0.47, and 0.50 kg m^{-2}) and snowfall rates (0.32, 0.19, 0.20, and 0.15 mm h^{-1}) than the monthly event-based averages.

In mid-March–April, the atmospheric freezing levels begin to rise in elevation as spring sun emerges to begin the thaw season; however, there are still several significant snowfall events. Monthly averages of column-integrated LWC and SLW are elevated in MA in comparison with DJF (Fig. 8). Excluding event 62 in early March, which has similar characteristics to the larger DJF events, MA has 4 events (72, 78, 81, and 86) with spatially averaged snowfall accumulations that exceed 7.5 mm; the largest occurring during 86. Event 72 was 51 h long with average column-integrated SLW of 0.38 kg m^{-2}, which is slightly lower than the monthly average in March. However, event 72 had a very large areal cloud coverage (74%) and yielded an average snowfall rate of 0.24 mm h^{-1}. The remaining events (78, 81, and 86) between mid-March and April all had significant levels of column-integrated SLW (0.59, 0.56, and 0.48 kg m^{-2}) and areal coverages of approximately 45%. However, the duration of event 86 was much longer (136 h) relative to events 78 and 81 (52 and 46 h, respectively) resulting in snowfall rates of 0.24, 0.18, and 0.2 mm h^{-1}, respectively. Although event 74 on 2 April does not have the highest snow accumulations, the event has the largest peak SLW (~0.04 g m^{-3} between 6 and 7 km) and largest column-integrated SLW (0.97 kg m^{-2}) with an areal coverage of liquid-containing columns of <20% during the event indicative of a short (6 h) convective event producing localized enhanced LWC resulting in spatially averaged snowfall of only 0.77 mm.

The event with the highest spatially averaged snowfall (28.8 mm) occurred on 7 January (event 45) with an areal coverage of liquid-containing columns of 54% and a column-integrated LWC of approximately 0.47 kg m^{-2}. It is possible that these longer significant snowfall events are associated with larger-scale sustained moisture flow patterns akin to inland atmospheric rivers, which were more common during December through early March during the 2016/17 winter season (Cann and Friedrich 2020). In addition to their extended duration and SLW coverage, no significant snowfall event (>5 mm) had an areal coverage of liquid-containing columns less than 40% of the domain, and most had >50%.

e. *IWC and snowfall*

The efficiency of a cloud turning SLW into frozen precipitation also depends on the ice crystal concentration as clouds with high SLW and high IWC are more efficient in generating snowfall than clouds that lack one or the other. The presence of significant SLW in icy clouds can lead to significant ice crystal growth at the expense of the available SLW via riming. Here, we analyze the IWC, accounting for all of the ice hydrometeors in the cloud that can lead to surface snowfall, which varies throughout the season in a similar seasonal pattern as SLW (Figs. 8 and 9). Higher levels of column-integrated IWC (Fig. 9) occur in October, March, and April, with monthly averages from 0.52 to 0.89 kg m^{-2}. November, December, and February have similar levels of IWC (~0.38 kg m^{-2}), with January having the lowest levels on average (0.28 kg m^{-2}). The highest IWC occurs in October despite this being a month with low snowfall accumulation (6% of seasonal total). This is mainly due to the short duration of the events in October (average 12.5 h as compared with the annual average of 26.6 h; Table 1) and the presence of snow and rain mixtures with ice crystals only reaching the ground at higher elevations and likely melting into raindrops at lower elevations. Following the SLW discussion in section 3d, here we highlight the most impactful snowfall events that occurred in December through early March. The relationship between IWC and snowfall accumulation (Fig. 9) is stronger than that for LWC and snowfall accumulation (Fig. 8) during the peak winter months: the r of column-integrated IWC and snowfall amounts is poor for the entire season is 0.11 ($p = 0.31$) but increases significantly to 0.68 ($p = 1.9 \times 10^{-5}$) for events in DJF. The areal coverage of ice-containing columns (green dotted line in Fig. 9) is virtually identical to the areal coverage of liquid-containing columns from Fig. 8; both of which are indicative of cloud cover capable of producing precipitation.

In December, there are 6 events that produced spatially averaged snowfall accumulations of >5 mm (events 30, 32, 34, 36, 37, and 38). Those 6 events have column-integrated averages of IWC between 0.35 and 0.65 kg m^{-2}, and all but one (event 37) have a higher column-integrated IWC than the

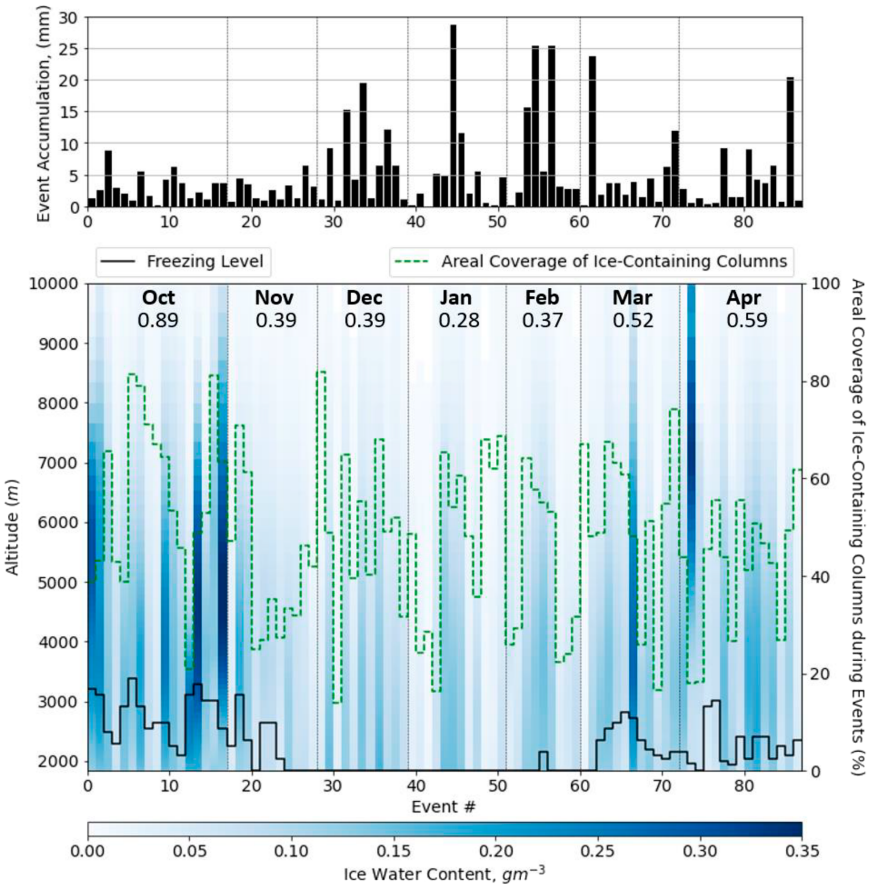

FIG. 9. (top) Spatially averaged snowfall accumulation per event averaged only where snowfall is occurring. (bottom) Domain-averaged IWC for each event as a function of height (shading) excluding grid cells with liquid water mixing ratios <0.001 g kg^{-1} below 10 km MSL (contains 95% of IWC). Domain and event-average height of the 0°C isotherm (solid black line), and areal coverage of liquid-containing clouds (dotted green line) are highlighted. Monthly event average column-integrated IWC (kg m^{-2}) up to 10 km is shown as text values.

monthly average for December (0.39 kg m^{-2}). The other 5 events in December with snowfall accumulations of <5 mm have column-integrated averages of IWC between 0.11 and 0.40 kg m^{-2}, and all but one (event 35) of those 5 events had a lower column-integrated IWC than the monthly average for December. This relationship is evident in the "every other" IWC pattern for events during December (Fig. 9). The same is true for January and February ($r = 0.69$, $p = 4.8 \times 10^{-4}$), where the events with high IWC (clustered in the middle of the two months) are correlated with higher snowfall event totals. The significant early March event (62) is similar to events seen in January and February than it is to the rest of the events in March. Its average surface temperature was below 0°C, its duration was 157 h, column-integrated SLW and IWC are 0.50 and 0.40 kg m^{-2}, respectively, and an approximately 50% domain coverage.

f. IWC, SLW, and snowfall

As has been illustrated previously, both SLW and IWC can be important and are correlated with peak winter snowfall. The ratio between column-integrated IWC and SLW, shown for all events between October and April in Fig. 10, illustrates the difference between solid versus liquid hydrometeors, which we use as a proxy for the efficiency of a cloud to produce snowfall with its SLW. If an event has a higher ratio of IWC to SLW, this suggests that the precipitation production is relatively efficient at transitioning liquid into ice or there was minimal SLW to begin with. A lower ratio suggests that there is still availability of SLW that has not been converted into IWC. Thus, clouds that are relatively inefficient at transitioning liquid into ice will maintain a high SLW content. With respect to cloud seeding, perhaps the events with lower IWC-to-SLW ratios that also have high SLW could be enhanced through seeding as there could be a dearth of ice-nucleating particles leading to inefficient SLW to IWC transitions.

The early and shoulder seasons, especially October, tend to have elevated IWC-to-SLW ratios. Since SLW content during those months is often > 0.4 kg m^{-2} (Fig. 8), these storms are technically "efficient" in converting the SLW into IWC but are more likely to have any frozen precipitation melt on the

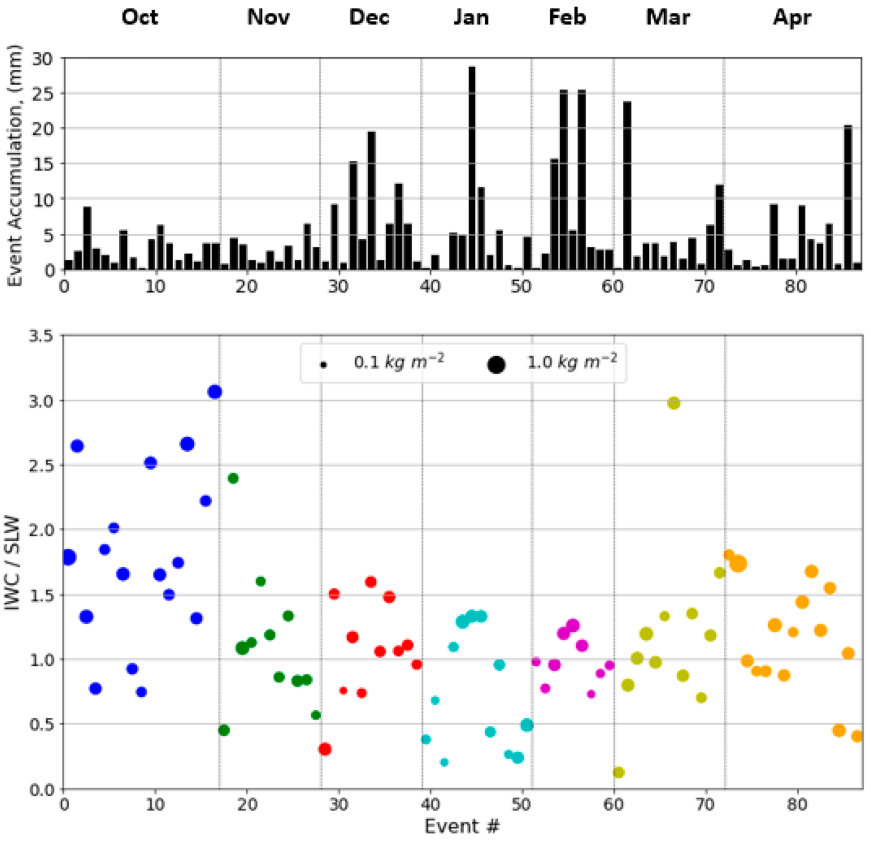

FIG. 10. (top) Spatially averaged snowfall accumulation per event averaged only where snowfall is occurring. (bottom) Scatterplot of the ratio of mean event column-integrated IWC to mean event column-integrated SLW. The size of the dots is related to the amount of mean event column-integrated SLW, and the colors indicate different months.

way to the ground except at high elevations. Despite higher IWC-to-SLW ratios in the early and shoulder seasons, events with >10 mm of snowfall mainly occurred December–early March (where IWC-to-SLW ratios range between 0.2 and 1.7). Of the 11 events with >10 mm of snowfall, 9 have IWC-to-SLW ratios > 1, and none have ratios < 0.5. However, one of the largest events of the season (event 62) has a ratio of 0.8 but produces snowfall accumulations of >23 mm. All 11 events also have column-integrated SLW totals > 0.3 kg m^{-2}. On the other end of the spectrum, events 29, 47, and 51 are notably inefficient in turning their ample SLW (0.51, 0.32, and 0.51 kg m^{-2}, respectively) into IWC, having IWC-to-SLW ratios of <0.5 and incurring < 5 mm of snowfall while lasting 12, 33, and 30 h, respectively. In addition to the column-integrated SLW and the IWC-to-SLW ratio, the event duration, spatial coverage of snowfall, and surface temperature affect the snowpack contribution as well.

g. *Cloud-seeding potential*

Cloud seeding seeks to enhance snowfall by contributing ice nucleating particles (INPs)—often silver iodide (AgI)—into clouds to aid the transition of SLW to snow and ice content (Ludlam 1955). Cloud-seeding operators generally seed every event possible especially in the coldest months of winter, but we would like to know the relative number of inefficient versus efficient events throughout the season to improve our understanding of the potential benefits that cloud seeding can provide to snowpack development. High levels of SLW and low values of IWC to SLW indicate an event is more likely to be enhanced through seeding of additional ice-nucleating particles than one where there is already elevated IWC. Since most events throughout the season are seeded in a normal cloud-seeding operation schedule, perhaps there are events throughout the season that could provide evidence to stakeholders of the need for attempting enhancement through seeding—that is, those events that have significant column-integrated SLW (>~0.35 kg m^{-2}) but fail to produce significant snowfall contributions (<10 mm). While there are a few of these events that occur in peak winter (DJF, blue dots in Fig. 11), there are several more events in the shoulder season (NMA, orange dots in Fig. 11) that are also prime candidates for seeding, especially if surface temperatures are close to or below freezing. These findings suggest that ~30% of the events in DJF are relatively inefficient—i.e., those with enough column-integrated SLW (>0.3 kg m^{-2}) and minimal snowfall accumulations (<10 mm).

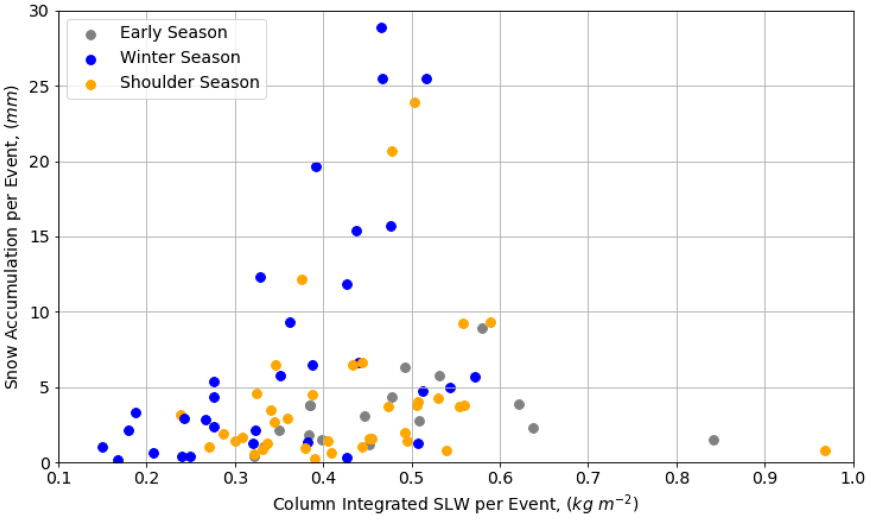

FIG. 11. Scatterplot of mean event column-integrated SLW to spatially averaged snowfall accumulation per event averaged only where snowfall is occurring for the peak winter months (DJF; blue), the shoulder seasons (NMA; green), and early season (October; gray).

4. Conclusions

This paper analyzes the seasonal snowfall characteristics of the central Idaho mountains between 1 October 2016 and 30 April 2017 using hourly 900-m WRF simulations output. The goal is to highlight the degree of temporal and spatial variability of snowpack production for this region and relate snowfall amount and distribution to thermodynamic and microphysical properties. Results from this analysis can be summarized as follows:

- The southwestern and western slopes of the Payette and Sawtooth Mountain ranges receive much higher levels of snowfall (>1.2 m) than do the similarly high elevation terrain to the east (<1 m), signifying a connection with the primarily westerly and southwesterly background flows that bring moisture to the region.
- Seasonal temperature evolution also plays a large role in where snowfall that falls is able to remain as snow and add to snowpack resources. Precipitation events in the early and shoulder seasons (ONMA) have higher T (>0°C on average at the surface) and SLW (average of 0.44 kg m^{-2} over the four months) than do events in peak winter (DJF, surface $T < -5$°C, SLW of 0.35 kg m^{-2}), but do not lead to as much snow on the ground except for at higher elevations.
- Efficient snowfall events follow a similar pattern: of the 11 of 87 snowfall events in the 2016/17 winter season with significant snowfall accumulation (>10 mm), 10 had high sustained column-integrated SLW and IVT (>0.35 kg m^{-2}), 9 had higher IWC-to-SLW ratios (>1), all had areal coverages of liquid-containing columns near or exceeding 50% of the domain, and 9 had freezing surface temperatures.
- Inefficient snowfall events [i.e., snowfall events that fail to produce significant snowfall (<10 mm) but that have significant SLW (>0.35 kg m^{-2})] are relatively common throughout the season (48 total events; 55% of seasonal events), even in DJF (10 events; 31% of peak winter events). For such events, cloud-seeding operators could be able to make a significant impact on snowpack production and to the water resources of the region.

Acknowledgments. This research is supported under NSF Grant AGS-2015829. The WRF simulations and subsequent analyses used in this study were completed on the NCAR/CISL HPCs, Cheyenne and Casper. The National Center for Atmospheric Research is sponsored by the National Science Foundation.

Data availability statement. WRF Model output are available for research purposes upon request (contact: Lulin Xue at xuel@ucar.edu). Code needed to run the analysis of the WRF Model output and to create the figures shown in this paper can be found online (https://github.com/mpw4rms/warms_et_al_2023_snowie_ams).

APPENDIX

WRF Model Validation with SNOTEL

a. Observational data

A validation of the high-resolution WRF Model reanalyses to SNOTEL stations was completed as part of the SNOWIE project (Tessendorf et al. 2018) using the model validation method from Rasmussen et al. (2011). Data from 16 SNOTEL sites (Fig. A1) in the central Idaho mountains and 21 sites from the eastern Idaho and upper Snake River region were used for the evaluation. The SNOTEL data from 1981 to present, where available, were inspected for quality control purposes using target and control sites and to determine whether there was a noticeable trend in seasonal precipitation with (2003–present) and without seeding (1981–2002) operations.

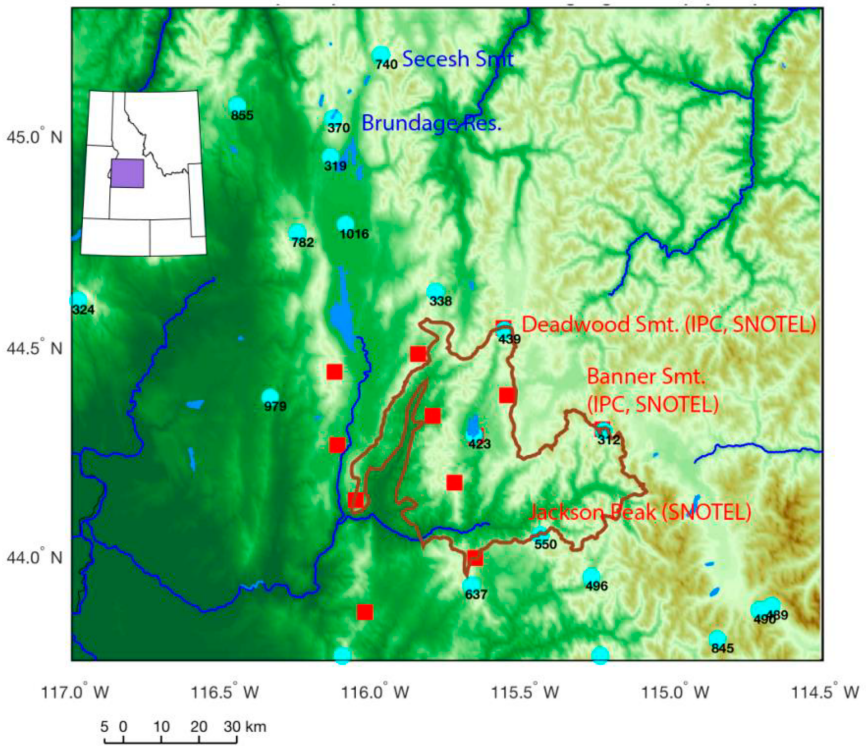

FIG. A1. Locations of central Idaho SNOTEL sites (cyan circles) and Idaho Power Company monitoring sites (red squares) in the central Idaho mountains that are used for model validation. All eastern Idaho SNOTEL sites, beginning after identifier 845 (bottom right), are not shown. Control (blue font) and target (red font) sites are used in data quality control. Numbers at SNOTEL sites are station identifiers used by the Natural Resources Conservation Service (Tessendorf et al. 2018; National Water and Climate Center 2022).

Results from the quality control analysis found that certain sites were susceptible to higher-than-average winds (>5 m s^{-1}) on a few occasions throughout the season, but no sites contained glaring inaccuracies.

b. SNOTEL vs WRF Model comparison

The validation study found that the WRF Model reproduces total seasonal snowpack evolution within 5% of total SNOTEL precipitation for the central Idaho mountains (Fig. A2a) and within 10% for the eastern Idaho mountains (Fig. A2b), capturing both the total and spatial distribution of snowfall in comparison with observations for the 2016/17 winter season. Most importantly for this study, each individual snowfall event was captured in the reanalysis, and high-elevation snowfall is modeled satisfactorily (within 10%).

The WRF Model output was also compared with the mean, minimum, and maximum surface temperatures at all 37 SNOTEL sites. As a model reanalysis, the WRF winds and temperatures are driven by the initial and boundary conditions that were obtained from the ERA-Interim dataset (31-km horizontal resolution; ECMWF 2011). On average, the WRF Model is slightly cooler than observations for all temperatures at high elevations—<2°C for mean and minimum temperatures and <4°C for maximum temperatures (Fig. A3)—and captures the seasonal and diurnal cycles well for the 2016/17 season. The complete model validation can be found be found in Tessendorf et al. (2018).

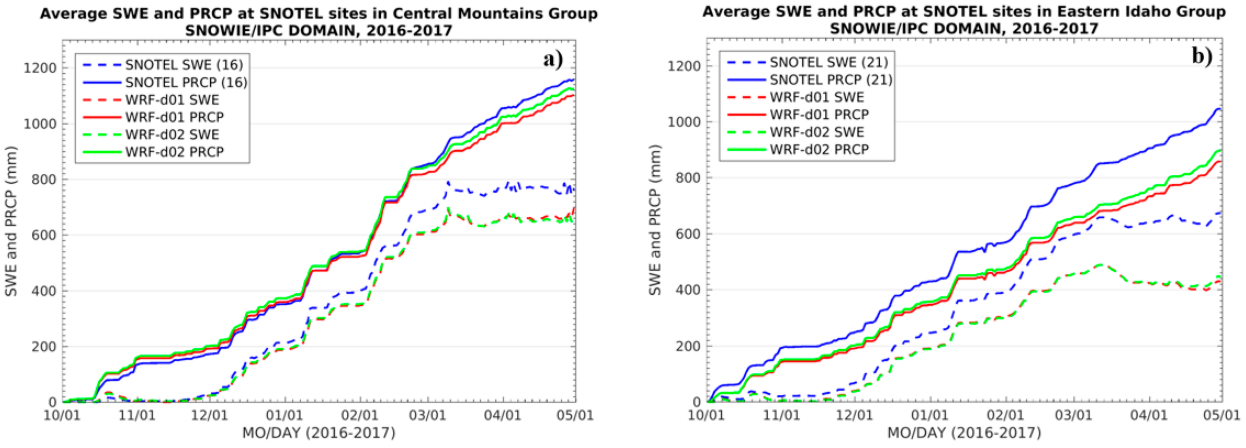

FIG. A2. SNOTEL (blue lines) vs WRF Model simulation (red for outer domain, green for inner domain) accumulation precipitation (solid lines) and SWE (dashed) values for the 2016/17 winter season for the (a) central mountains and (b) eastern Idaho regions (Tessendorf et al. 2018).

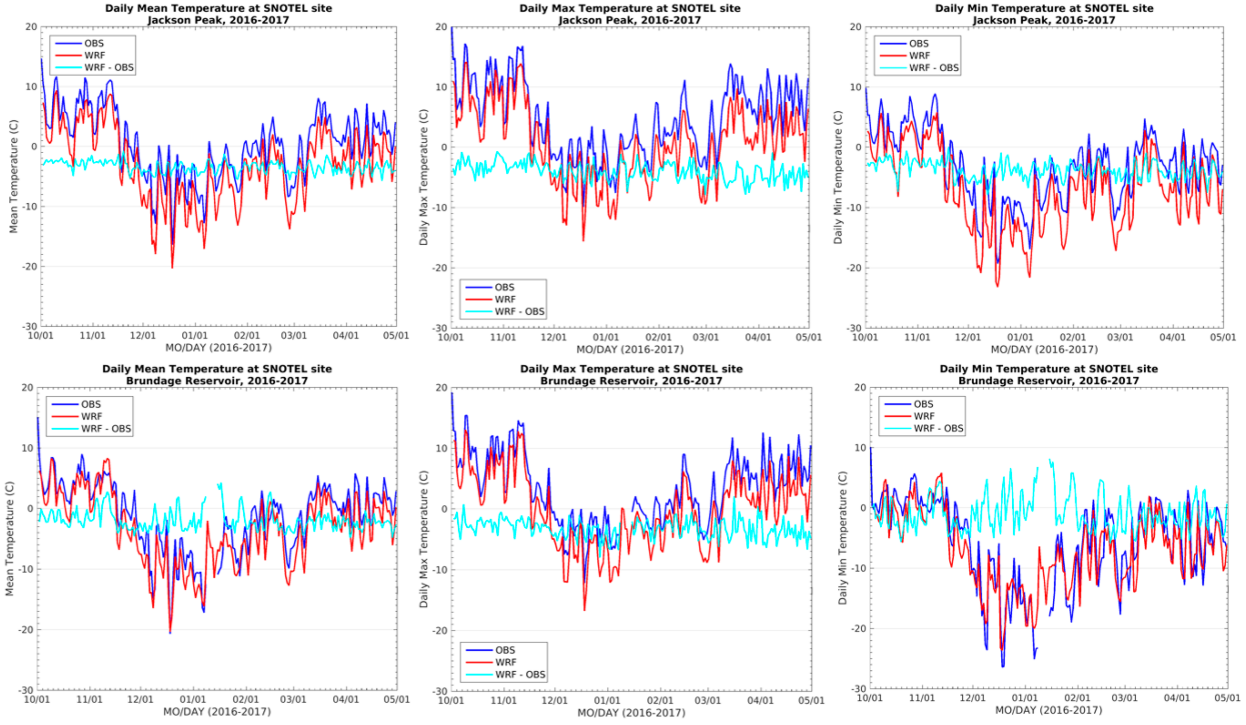

FIG. A3. SNOTEL (blue) vs WRF (red) model-simulated (left) mean, (center) maximum, and (right) minimum temperatures for the 2016/17 winter season at (top) Jackson Peak and (bottom) Brundage Reservoir (Tessendorf et al. 2018). These comparisons were completed for all 37 SNOTEL locations.

REFERENCES

Alexander, M. A., J. D. Scott, D. Swales, M. Hughes, K. Mahoney, and C. A. Smith, 2015: Moisture pathways into the U.S. Intermountain West associated with heavy winter precipitation events. *J. Hydrometeor.*, **16**, 1184–1206, https://doi.org/10.1175/JHM-D-14-0139.1.

Barlow, M., and Coauthors, 2019: North American extreme precipitation events and related large-scale meteorological patterns: A review of statistical methods, dynamics, modeling, and trends. *Climate Dyn.*, **53**, 6835–6875, https://doi.org/10.1007/s00382-019-04958-z.

Cann, M. D., and K. Friedrich, 2020: The role of moisture pathways on snowfall amount and distribution in the Payette Mountains of Idaho. *Mon. Wea. Rev.*, **148**, 2033–2048, https://doi.org/10.1175/MWR-D-19-0350.1.

Chen, F., and Coauthors, 2014: Modeling seasonal snowpack evolution in the complex terrain and forested Colorado headwaters region: A model intercomparison study. *J. Geophys. Res. Atmos.*, **119**, 13 795–13 819, https://doi.org/10.1002/2014JD022167.

Dettinger, M., B. Udall, and A. Georgakakos, 2015: Western water and climate change. *Ecol. Appl.*, **25**, 2069–2093, https://doi.org/10.1890/15-0938.1.

Dudley, R. W., G. A. Hodgkins, M. R. McHale, M. J. Kolian, and B. Renard, 2017: Trends in snowmelt-related streamflow timing in the conterminous United States. *J. Hydrol.*, **547**, 208–221, https://doi.org/10.1016/j.jhydrol.2017.01.051.

ECMWF, 2011: The ERA-Interim reanalysis dataset. Copernicus Climate Change Service, accessed 1 April 2018, https://www.ecmwf.int/en/forecasts/datasets/archive-datasets/reanalysis-datasets/era-interim.

French, J. R., and Coauthors, 2018: Precipitation formation from orographic cloud seeding. *Proc. Natl. Acad. Sci. USA*, **115**, 1168–1173, https://doi.org/10.1073/pnas.1716995115.

Friedrich, K., and Coauthors, 2020: Quantifying snowfall from orographic cloud seeding. *Proc. Natl. Acad. Sci. USA*, **117**, 5190–5195, https://doi.org/10.1073/pnas.1917204117.

Fukuta, N., and T. Takahashi, 1999: The growth of atmospheric ice crystals: A summary of findings in vertical supercooled cloud tunnel studies. *J. Atmos. Sci.*, **56**, 1963–1979, https://doi.org/10.1175/1520-0469(1999)056<1963:TGOAIC>2.0.CO;2.

Iacono, M. J., J. S. Delamere, E. J. Mlawer, M. W. Shephard, S. A. Clough, and W. D. Collins, 2008: Radiative forcing by long-lived greenhouse gases: Calculations with the AER radiative transfer models. *J. Geophys. Res.*, **113**, D13103, https://doi.org/10.1029/2008JD009944.

Kharin, V. V., F. W. Zwiers, X. Zhang, and M. Wehner, 2013: Changes in temperature and precipitation extremes in the CMIP5 ensemble. *Climatic Change*, **119**, 345–357, https://doi.org/10.1007/s10584-013-0705-8.

Laiho, R., K. Friedrich, and A. C. Winters, 2023: Characteristics of warm season heavy rainfall in Minnesota. *Wea. Forecasting*, **38**, 163–177, https://doi.org/10.1175/WAF-D-21-0186.1.

Liu, X., F. Chen, M. Barlage, G. Zhou, and D. Niyogi, 2016: Noah-MP-Crop: Introducing dynamic crop growth in the Noah-MP land surface model. *J. Geophys. Res. Atmos.*, **121**, 13 953–13 972, https://doi.org/10.1002/2016JD025597.

Livneh, B., and A. M. Badger, 2020: Drought less predictable under declining future snowpack. *Nat. Climate Change*, **10**, 452–458, https://doi.org/10.1038/s41558-020-0754-8.

Ludlam, F. H., 1955: Artificial snowfall from mountain clouds. *Tellus*, **7**, 277–290, https://doi.org/10.3402/tellusa.v7i3.8908.

Mitchell, D. L., R. Zhang, and R. L. Pitter, 1990: Mass dimensional relationships for ice particles and the influence of riming on snowfall rates. *J. Appl. Meteor.*, **29**, 153–163, https://doi.org/10.1175/1520-0450(1990)029<0153:MDRFIP>2.0.CO;2.

Mote, P. W., A. F. Hamlet, M. P. Clark, and D. P. Lettenmaier, 2005: Declining mountain snowpack in western North America. *Bull. Amer. Meteor. Soc.*, **86**, 39–50, https://doi.org/10.1175/BAMS-86-1-39.

Nakanishi, M., and H. Niino, 2006: An improved Mellor–Yamada level-3 model: Its numerical stability and application to a regional prediction of advection fog. *Bound.-Layer Meteor.*, **119**, 397–407, https://doi.org/10.1007/s10546-005-9030-8.

National Water and Climate Center, 2022: Snow telemetry (SNOTEL) and snow course data and products. USDA Natural Resources Conservation Service, accessed 1 May 2023, www.wcc.nrcs.usda.gov/snow/index.html.

Niu, G.-Y., and Coauthors, 2011: The community Noah land surface model with multiparameterization options (Noah-MP): 1. Model description and evaluation with local-scale measurements. *J. Geophys. Res.*, **116**, D12109, https://doi.org/10.1029/2010JD015139.

O'Gorman, P. A., 2014: Contrasting responses of mean and extreme snowfall to climate change. *Nature*, **512**, 416–418, https://doi.org/10.1038/nature13625.

Ralph, F. M., J. J. Rutz, J. M. Cordeira, M. Dettinger, M. Anderson, D. Reynolds, L. J. Schick, and C. Smallcomb, 2019: A scale to characterize the strength and impacts of atmospheric rivers. *Bull. Amer. Meteor. Soc.*, **100**, 269–289, https://doi.org/10.1175/BAMS-D-18-0023.1.

Rasmussen, R. M., and Coauthors, 2011: High-resolution coupled climate runoff simulations of seasonal snowfall over Colorado: A process study of current and warmer climate. *J. Climate*, **24**, 3015–3048, https://doi.org/10.1175/2010JCLI3985.1.

Rauber, R. M., and L. O. Grant, 1986: The characteristics and distribution of cloud water over the mountains of northern Colorado during wintertime storms. Part II: Spatial distribution and microphysical characteristics. *J. Climate Appl. Meteor.*, **25**, 489–504., https://doi.org/10.1175/1520-0450(1986)025<0489:TCADOC>2.0.CO;2.

——, and Coauthors, 2019: Wintertime orographic cloud seeding—A review. *J. Appl. Meteor. Climatol.*, **58**, 2117–2140, https://doi.org/10.1175/JAMC-D-18-0341.1.

Rutz, J. J., W. J. Steenburgh, and F. M. Ralph, 2014: Climatological characteristics of atmospheric rivers and their inland penetration over the western United States. *Mon. Wea. Rev.*, **142**, 905–921, https://doi.org/10.1175/MWR-D-13-00168.1.

Stewart, I. T., D. R. Cayan, and M. D. Dettinger, 2005: Changes toward earlier streamflow timing across western North America. *J. Climate*, **18**, 1136–1155, https://doi.org/10.1175/JCLI3321.1.

Takahashi, T., T. Endoh, and G. Wakahama, 1991: Vapor diffusional growth of free-falling snow crystals between −3 and −23°C. *J. Meteor. Soc. Japan*, **69**, 15–30.

Tessendorf, S. A., and Coauthors, 2018: Idaho power cloud seeding: Phase seven study. NCAR Final Rep., 113 pp.

——, and Coauthors, 2019: A transformational approach to winter orographic weather modification research: The SNOWIE project. *Bull. Amer. Meteor. Soc.*, **100**, 71–92, https://doi.org/10.1175/BAMS-D-17-0152.1.

Thompson, G., and T. Eidhammer, 2014: A study of aerosol impacts on clouds and precipitation development in a large

winter cyclone. *J. Atmos. Sci.*, **71**, 3636–3658, https://doi.org/10.1175/JAS-D-13-0305.1.

U.S. Energy Information Administration, 2016: Idaho electricity profile 2016: Electric power industry generation by primary energy source, 1990 through 2016. Accessed 1 April 2023, https://www.eia.gov/electricity/state/archive/2016/idaho/.

——, 2022: Idaho electricity profile 2022: Electric power industry generation by primary energy source, 2022. Accessed 1 May 2023, https://www.eia.gov/state/analysis.php?sid=ID.

Xue, L., and Coauthors, 2022: Comparison between observed and simulated AgI seeding impacts in a well-observed case from the SNOWIE field program. *J. Appl. Meteor. Climatol.*, **61**, 345–367, https://doi.org/10.1175/JAMC-D-21-0103.1.